

AD-A076 251

STANFORD UNIV CA EDWARD L GINZTON LAB

F/G 17/1

RECOUNT OF PROGRAM ON ACOUSTIC MICROSCOPY AT STANFORD. ACOUSTIC--ETC(U)

1977 C F QUATE

N00014-75-C-0632

UNCLASSIFIED

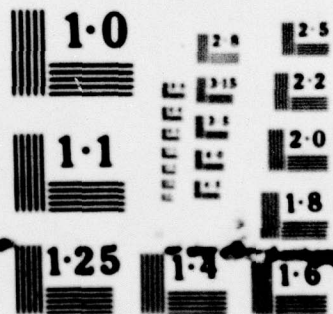
6L-2689

NL

1 OF 1  
AD-A076251



END  
DATE  
FILMED  
11-79  
DDC



NATIONAL BUREAU OF STANDARDS  
MICROCOPY RESOLUTION TEST CHART

FILE COPY

Edgemoor Laboratory

"RECOUNT OF PROGRAM ON ACOUSTIC MICROSCOPY

AT STANFORD"

C. F. Quate

2

G. L. Report No. 2689 ✓

Internal Memorandum

LEVEL II

Contract

NO0014-75-C-0632 ✓

and

NBS5-35899

DDC  
RECEIVED  
7 NOV 1979  
C

Acoustic Microscopy Symposium-Workshop

Indianapolis Center for Advanced Research,

Indianapolis, Indiana

February 14-18, 1977

APPROVED FOR PUBLIC RELEASE; DISTRIBUTION UNLIMITED

499640 ✓  
Edward L. Ginzton Laboratory  
W. W. Hansen Laboratories of Physics  
Stanford University  
Stanford, California

APRIL 1977

79 06 20 127

A076251

DDC FILE COPY

9 Internal name,,

14 GL-2689

12 24

6 RECOUNT OF PROGRAM ON ACOUSTIC MICROSCOPY  
AT STANFORD.

10  
C. F. Quate

11 1977

Acoustic Microscopy Symposium-Workshop,  
Indianapolis Center for Advanced Research,  
Indianapolis, Indiana,

February 14-18, 1977.

15  
NND714-75-C-0632, NBS3-35899

Accession For	
NTIS GRA&I	<input checked="checked" type="checkbox"/>
DOC TAB	<input type="checkbox"/>
Unannounced	<input type="checkbox"/>
Justification	
By _____	
Distribution/ _____	
Availability Codes	
Dist	Avail and/or special
A	

409 640

slt

## RECOUNT OF PROGRAM ON ACOUSTIC MICROSCOPY AT STANFORD

### I. BACKGROUND AND THE INITIAL EFFORT

↙  
The work at Stanford (Hansen Laboratories) began in the early sixties with an exploration of bulk acoustic waves in high-quality crystals such as Lithium Niobate and piezoelectric semiconductors such as Cadmium Sulphide. The work with Niobate was focused on acousto-optic interactions and a number of devices such as acousto-optic modulators and optical filters and surface wave convolvers have evolved from this initial work. It was the Zinc Oxide thin film transducer that allowed us to enter this domain of technology. We acquired the capacity to fabricate these transducers in a manner that gave us efficient conversion of electromagnetic energy into acoustic energy over a wide band of frequencies. It also permitted us to work at frequencies above 1000 MHz. In liquids the acoustic wavelength of 1.5 microns is in the neighborhood of optical wavelengths. It was natural to think about microscopes based on this form of radiation. Perhaps the resolution would equal or exceed the resolution of the optical instrument.

Since we were working with the acousto-optic interactions in  $\text{LiNbO}_3$  we based the design of our first instrument on this technique. This interaction enabled us to transfer the acoustic pattern to an optical pattern which could be recorded on photographic film. The first device is sketched in Fig. 1 and the first image of a rectangular grid is shown in Fig. 2. These initial results were certainly a beginning, but we recognized that the system was limited to a low numerical aperture. The resolution could not, therefore, be less than several wavelengths of sound. The velocity of sound is high in Niobate and, therefore, the acoustic wavelength for a given frequency is large. We did spend time on a compound lens to increase the numerical aperture but the complexity of this system in anisotropic crystals was too great.

In parallel with this we knew that the group at Zenith led by A. Karpel & L. Kessler and the group at Stanford with B. Auld were working on microscopes where the resolving power was determined by the wavelength of sound in the liquids - a factor of 4 to 6 below that of the wavelength in crystals. Those systems incorporated scanning optical beams in the readout system.

In our laboratory we redirected our efforts toward a second system as sketched in Fig. 3. We used the acoustic radiation pressure to rearrange small latex spheres into a pattern that reproduced the acoustic image. The distribution of spherical particles in this emulsion was observed through an optical microscope. A typical image is as shown in Fig. 4 where the resolution is at 900 MHz. The resolution in that image is 4 microns. This is twice the wavelength of sound - a far cry from the theoretical limit of  $\lambda/4$ .

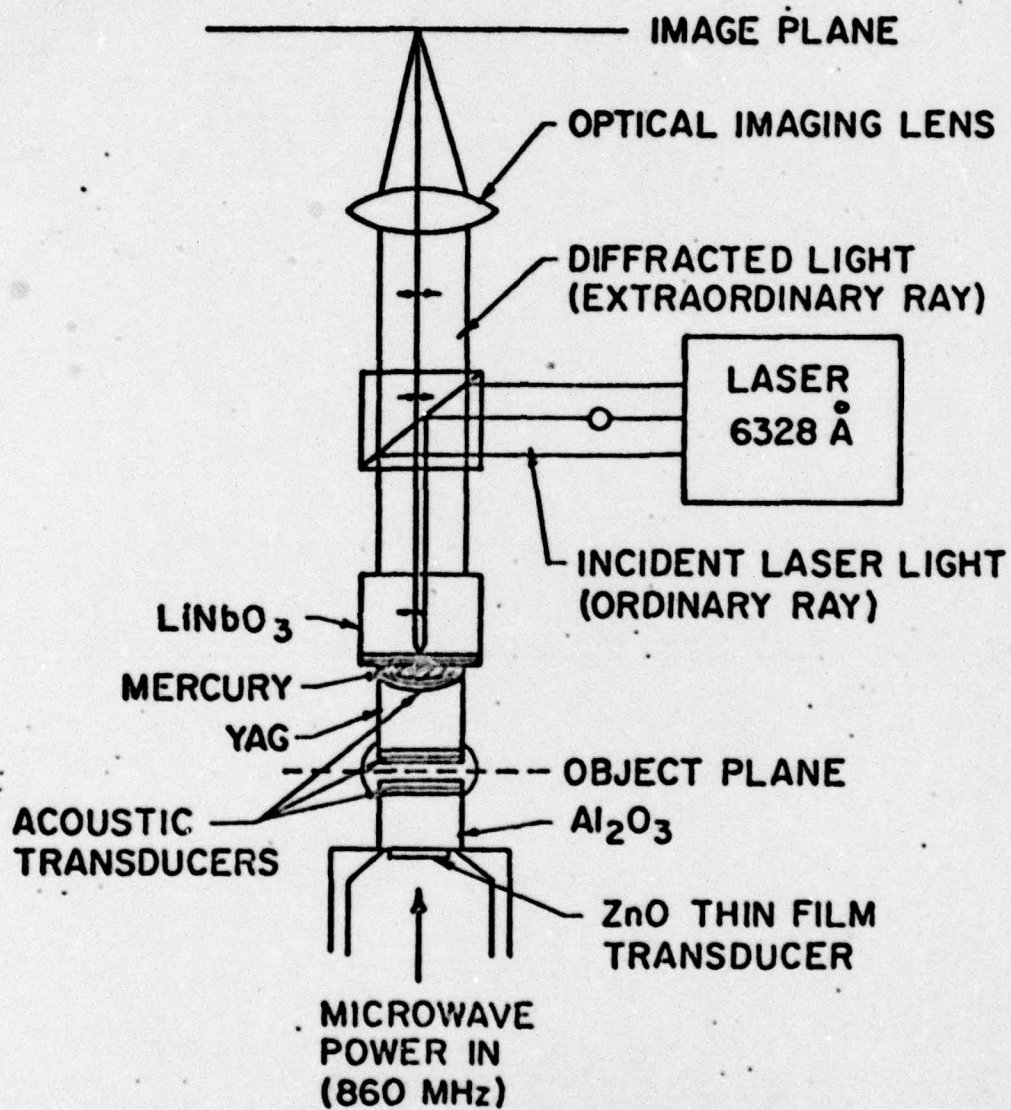


FIG. 1--Experimental setup

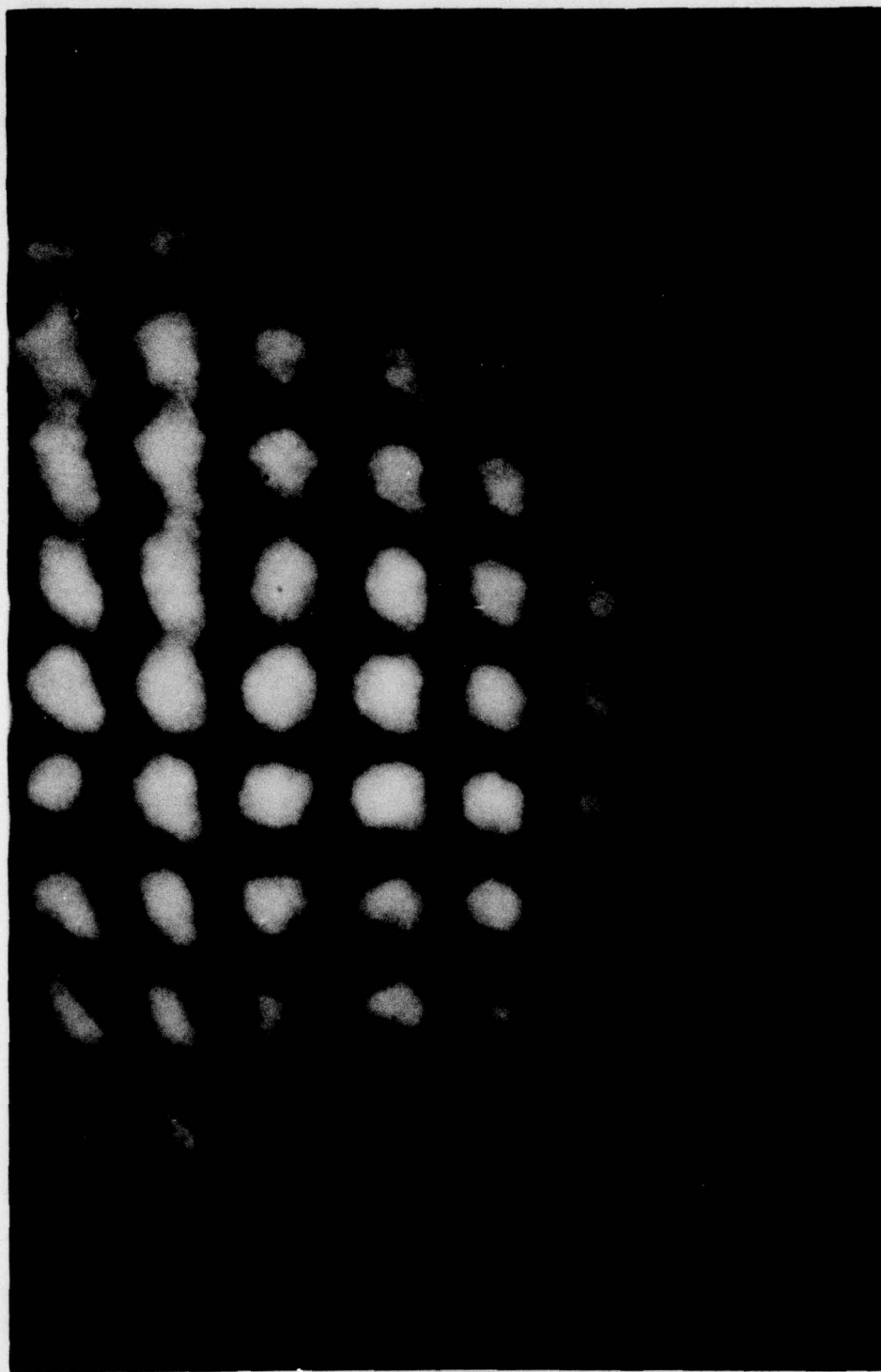


Image of 50  $\mu$  periodic mesh, in focus region

**Fig. 2**

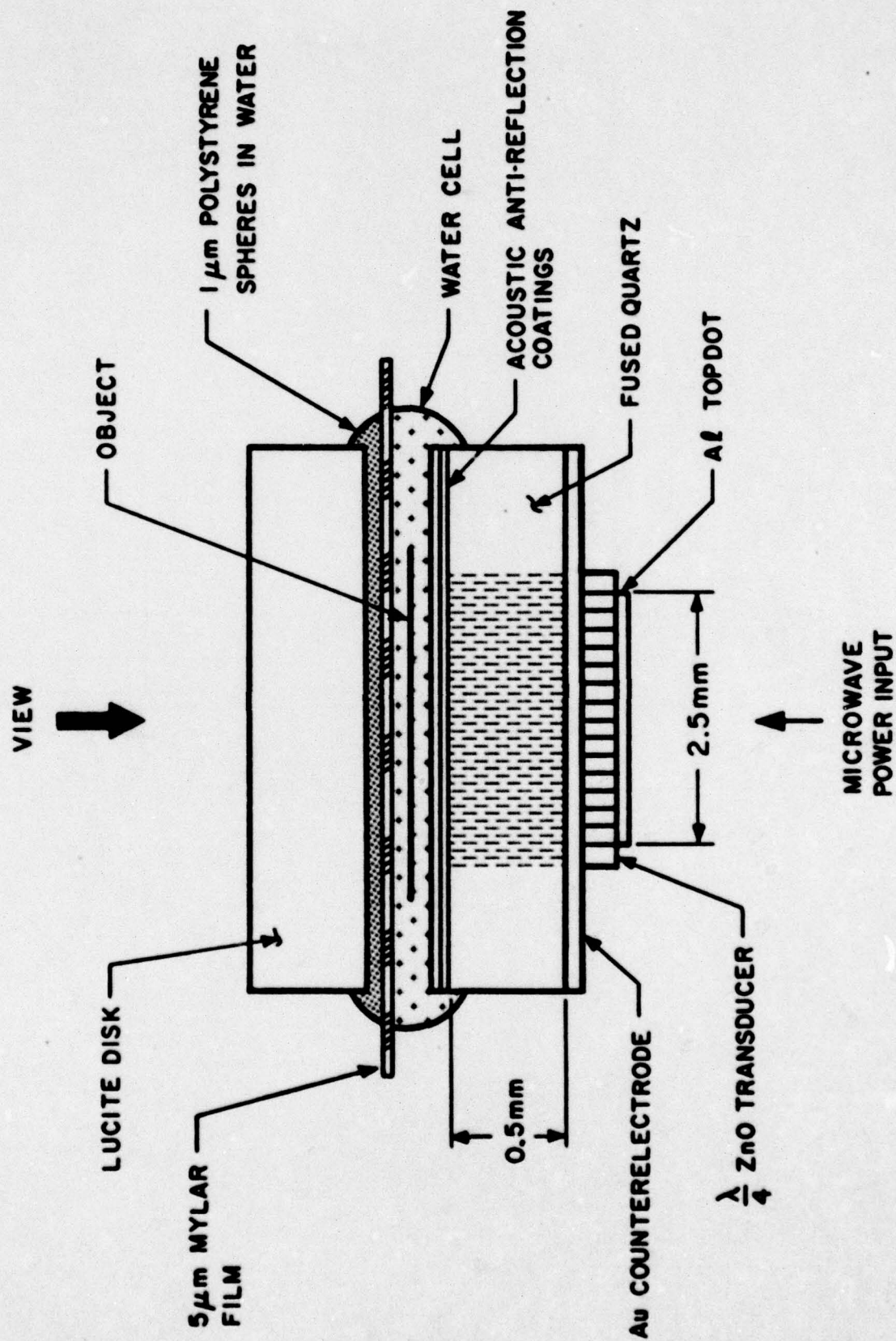
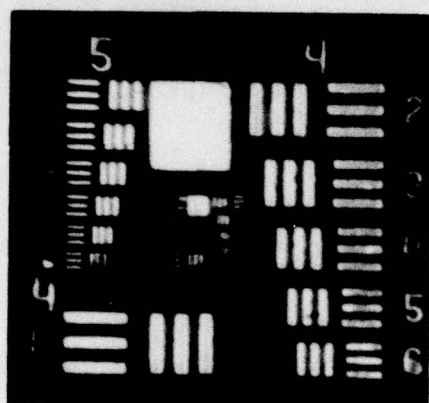
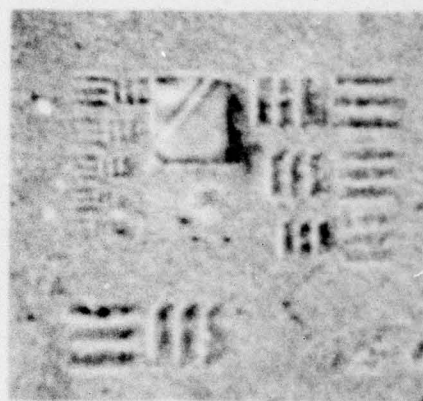


FIG. 3 Experimental arrangement for locating the object in the extremely near field of a large area transducer.



(a)



(b)

# USAF RESOLUTION CHART DATA

## GROUP +4

(1)	16.00	Li/mm
(2)	17.96	"
(3)	20.32	"
(4)	22.80	"
(5)	25.56	"
(6)	28.51	"

## GROUP +5

(1)	32.00	Li/mm
(2)	35.92	"
(3)	40.64	"
(4)	45.60	"
(5)	51.12	"
(6)	57.02	"

FIG. 4 1951 USAF Resolution Test Chart: Groups +4 and +5.

(a) Optical image; (b) Acoustic image.

The system suffered from the lack of magnification - it is essentially a contact printing system with unity magnification. We determined that the acoustic power would increase significantly as we increased the frequency to improve the resolution. And, as a final point, we could not find a method that would permit us to record images in reflection - a requirement for examining single surfaces. These deficiencies were sufficient to convince us that it would be necessary to explore new avenues. We began to devote a larger and larger fraction of our effort to the system that was based on mechanical scanning. There the object is translated through the narrow waist of a focused acoustic beam.

## II. THE SCANNING ACOUSTIC MICROSCOPE

As we began the work with the scanning system we soon came to realize that simple single surface lenses could be used to focus the acoustic beam into a diffracted limited waist. This fortunate circumstance reduced the complexity of the system and allowed us to fabricate a rather simple acoustic cell.

The components of this acoustic cell are sketched in Fig. 5. We want to stress the point that it is the large difference between the velocity in sapphire and in water that makes this form possible. The problem of spherical aberration does not arise - a point that is illustrated by the ray tracing sketch of Fig. 6. Without spherical aberration the ideal lens can be made with a single spherical surface. The diameter at the waist of this focused beam can be equal to a fraction of a wavelength since it is limited only by diffraction. At the same time we know that the field of view for

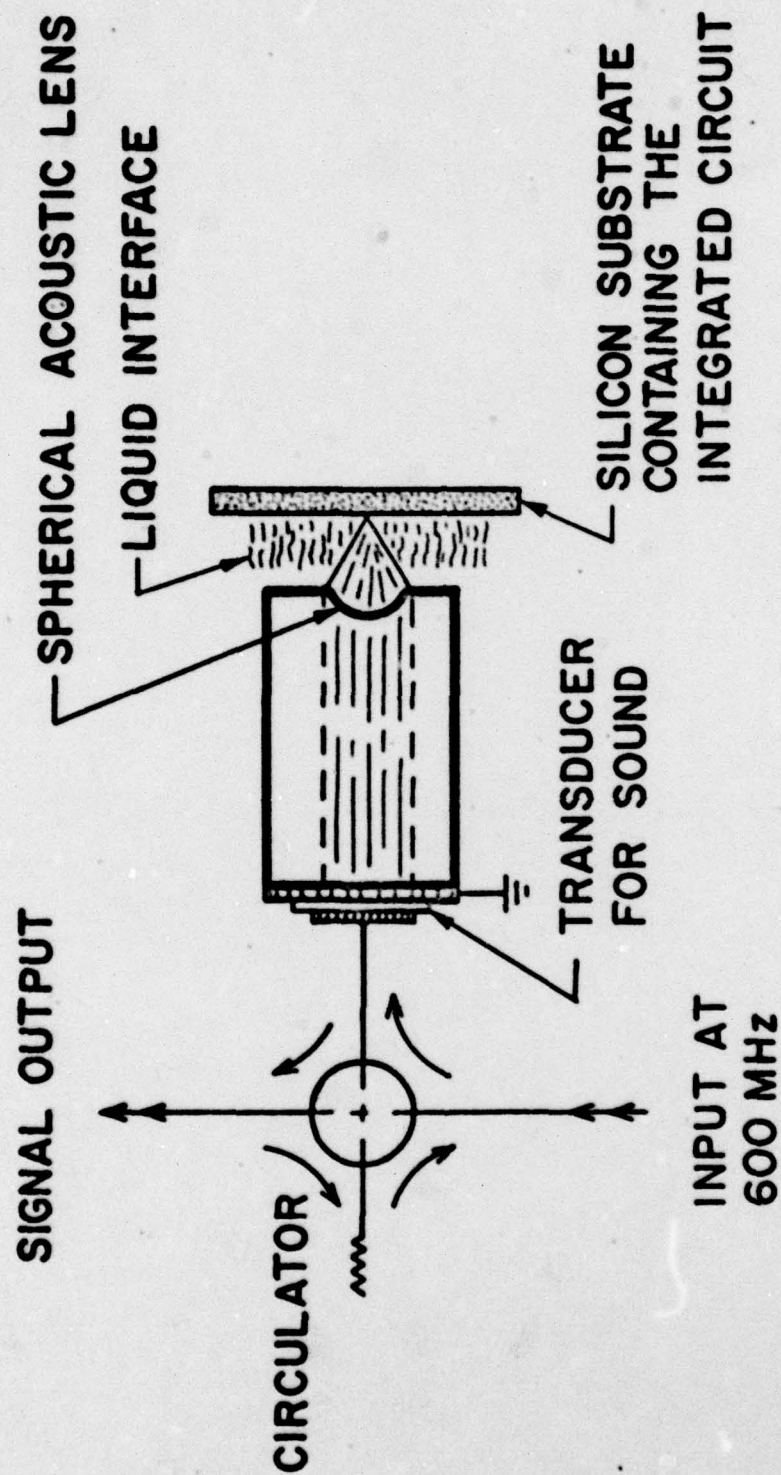


Fig. 5 Diagrammatic scheme for the Reflection Mode. The silicon substrate is scanned mechanically to obtain the image.

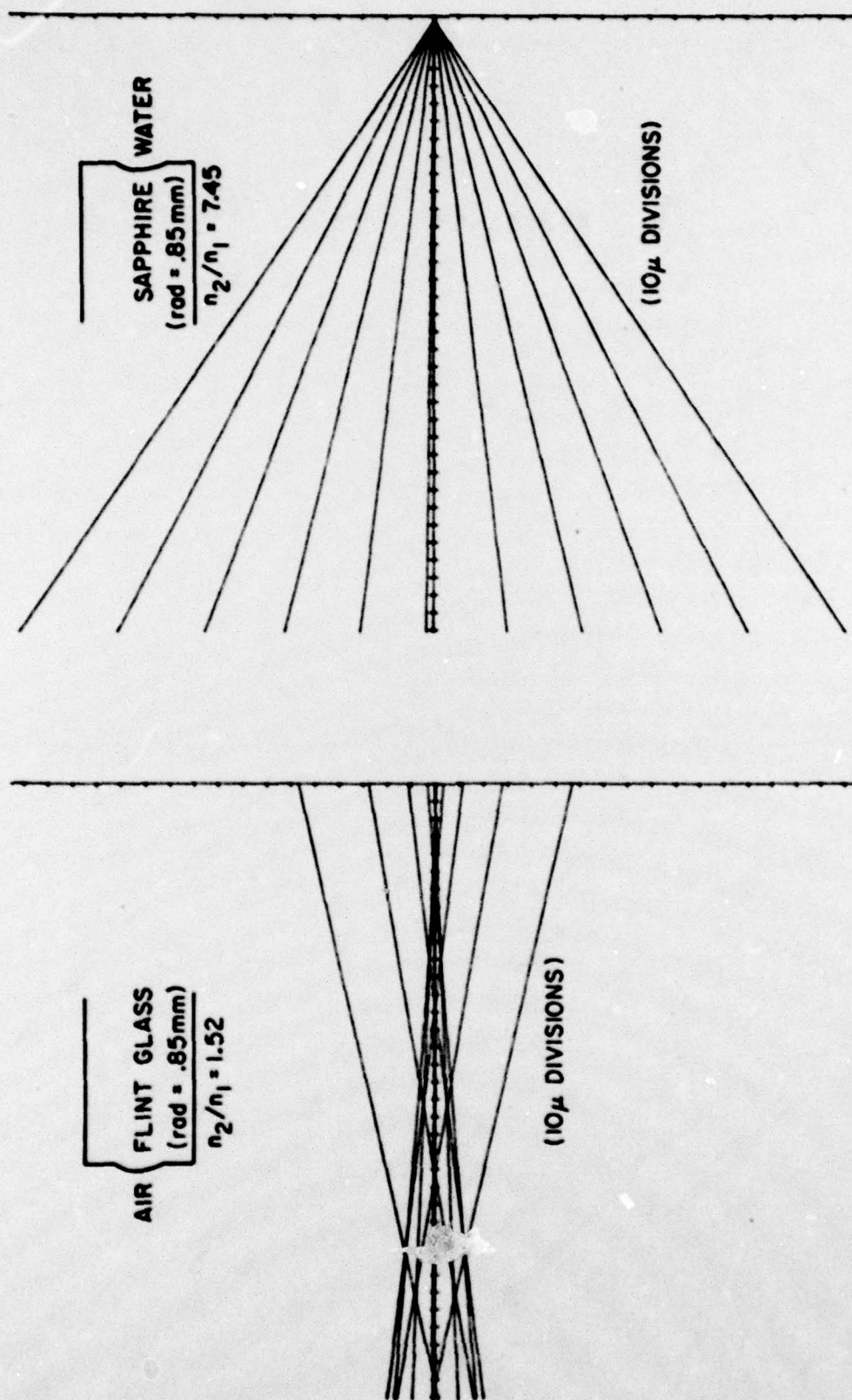


FIG. 6 Ray tracing comparison of the performance of a single surface lens in a light optical system (left) and an acoustic system (right). The paraxial focus lies at the ordinate.

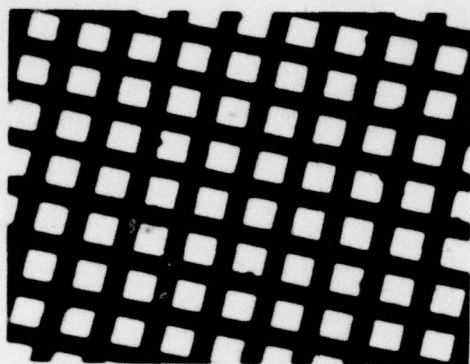
this highly focused beam is negligibly small but we can overcome this by using mechanical scanning to sequentially move the object through the beam waist.

The first image with the scanning instrument was recorded at 160 MHz where the wavelength in water is near 10 microns. The images of the grid and spheres as in Fig. 7 demonstrate that the resolution is less than 10 microns. This gave us courage to push toward higher frequencies.

We were able to generate images at 500 MHz in the second version and there the resolution is 2 microns ( $\lambda = 3$  microns). We also learned with this instrument that we could work in the reflection mode. The HP22 - a high frequency bipolar transistor - was the first object that was examined in this mode (Fig. 8). Another illustration is shown in Fig. 9.

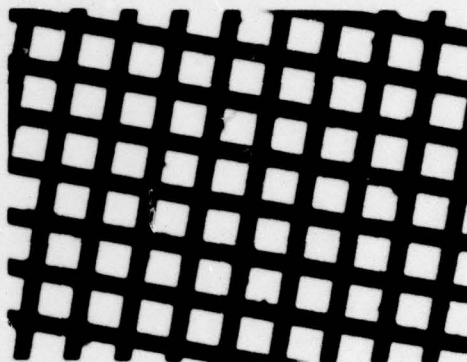
With images of these structures and the associated work with blood cells and fixed tissues we were able to obtain funding from both the National Science Foundation and the National Bureau of Standards. The NSF money was used to continue the work on instrumentation and to pursue the study of biological specimens. The NBS money was used to study the characteristics of silicon and silicon devices. The images of Fig. 10 and Fig. 11 were generated on that program and their quality is high enough to demonstrate some of the power of acoustic microscopy. The wafers and devices within the silicon-on-sapphire technology and the illustrations of Figs. 10 and 11 show the strong contrast that is possible in these devices. We believe this contrast will provide a method for detecting defects that is superior to present methods as based on optical observations.

ACOUSTIC  
IMAGE



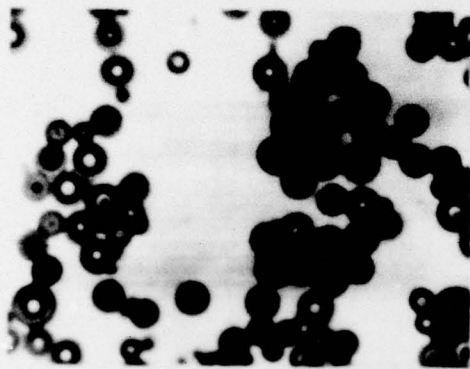
100  $\mu$ m

OPTICAL  
IMAGE

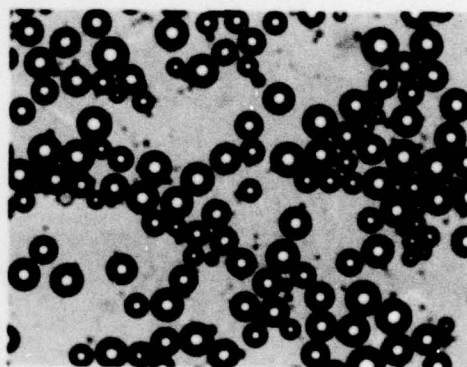


100  $\mu$ m

Comparison of the acoustic (left) and optical (right) images of a 500 mesh nickel grid.



100  $\mu$ m



100  $\mu$ m

Comparison of the acoustic (left) and optical (right) images of polystyrene particles.

Fig. 7

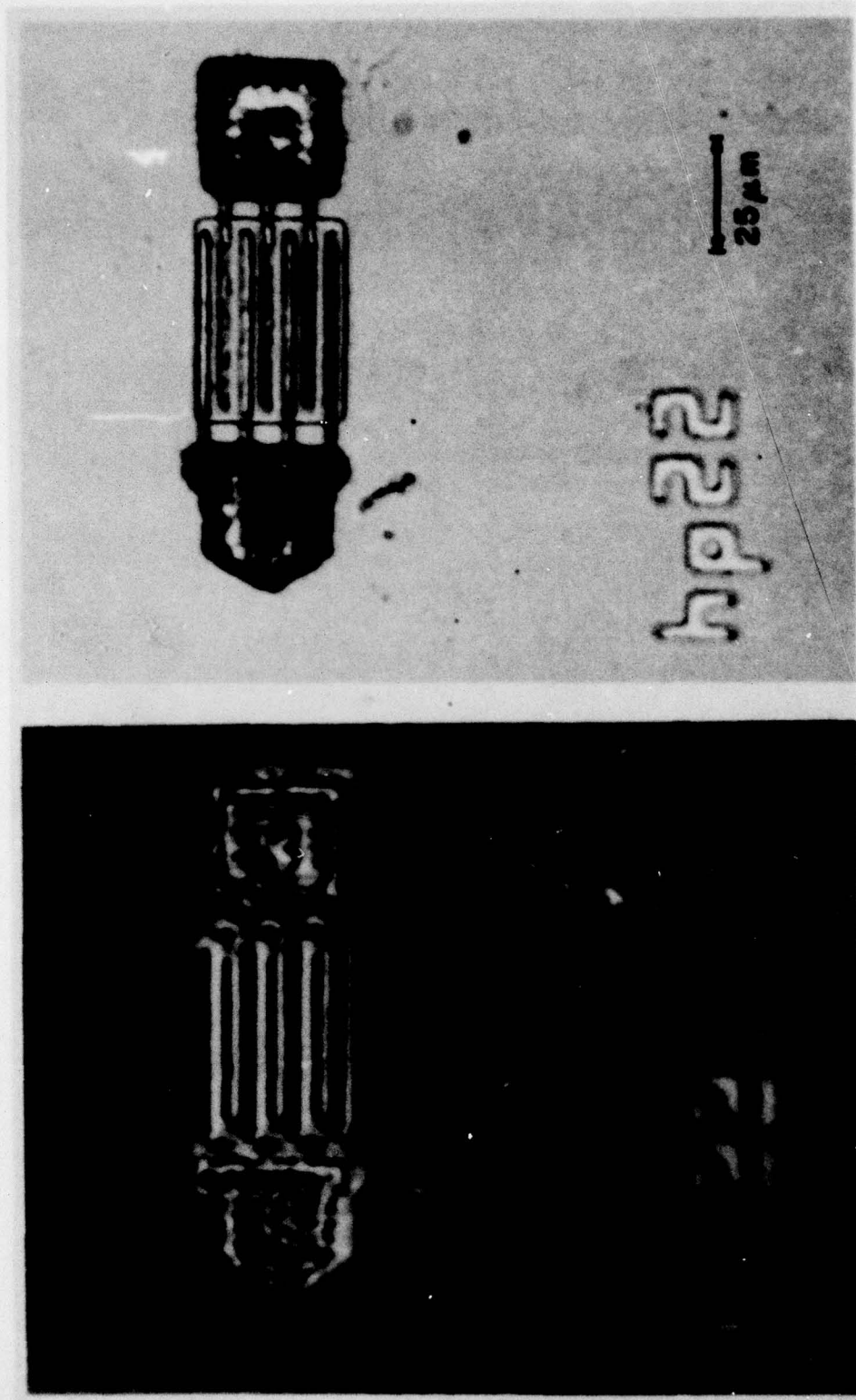


FIG. 8 --Acoustic (left) and Optical (right) reflection micrographs of a small bipolar transistor. The width of the three narrow fingers is 2 microns.

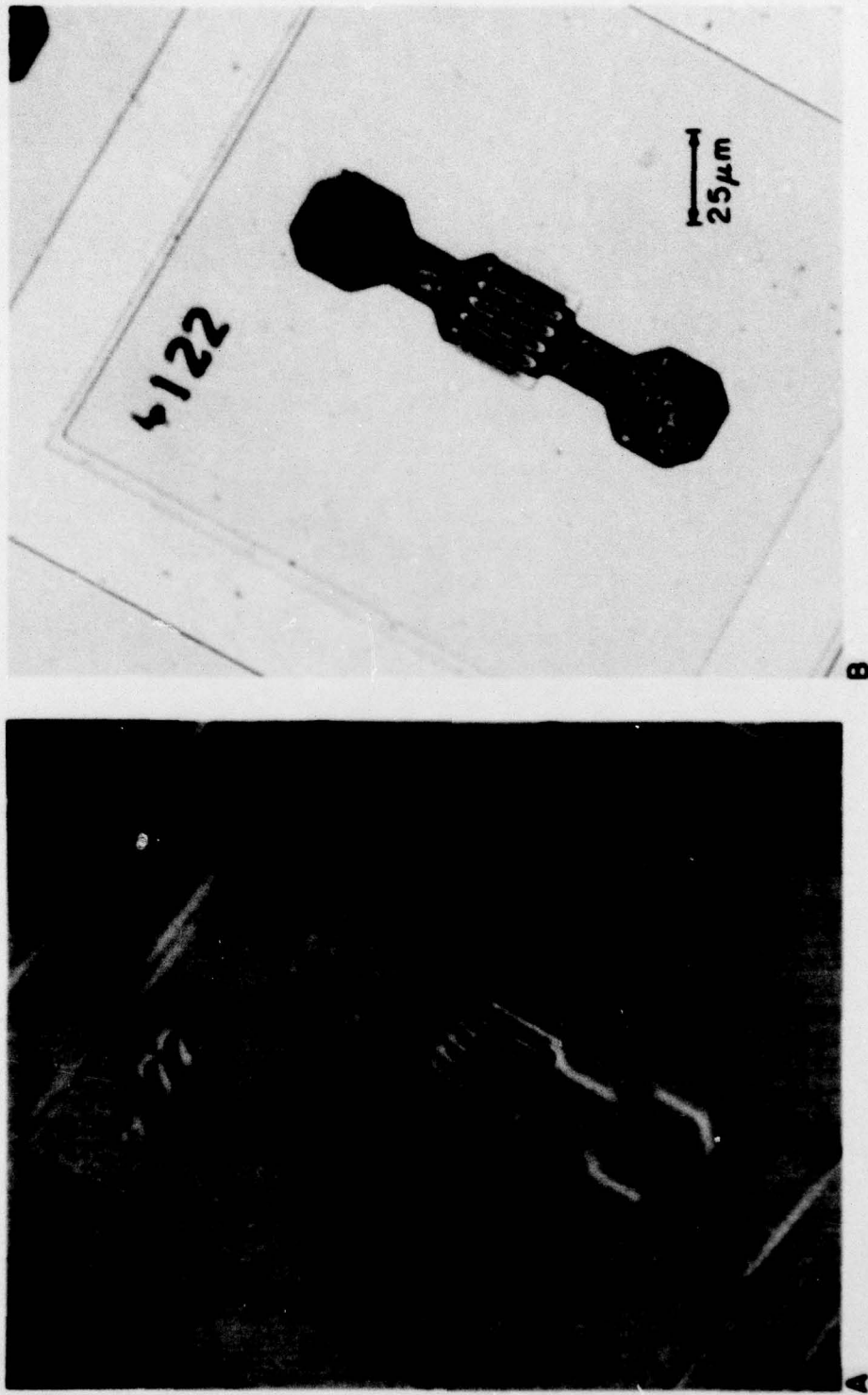
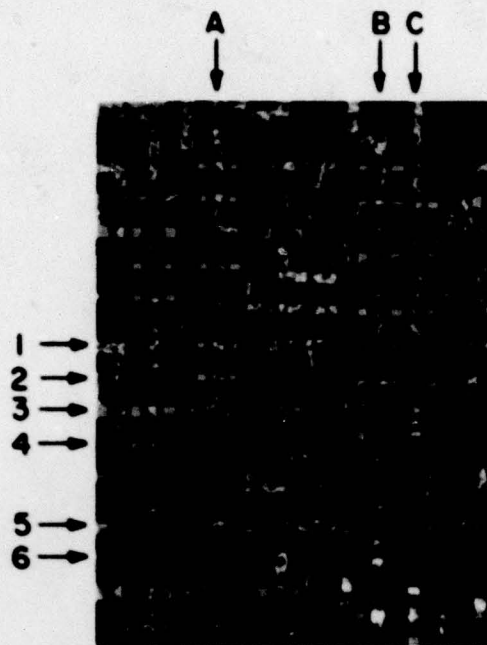
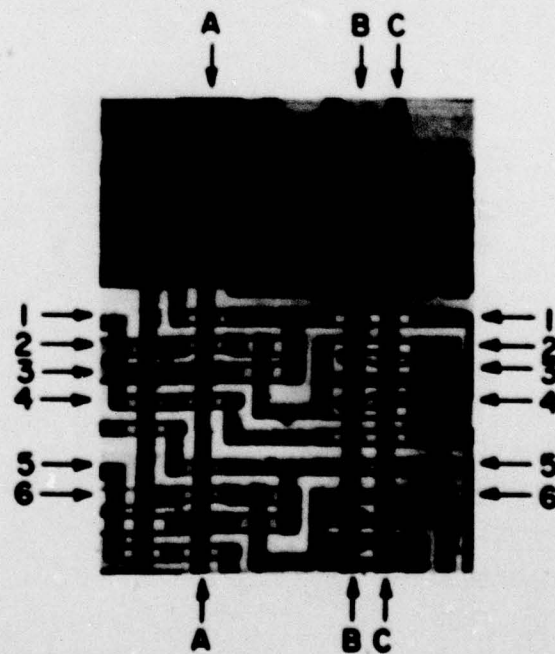


Fig. 9 A comparison between the acoustic (A) and optical (B) images of the hpl22--a high frequency bipolar transistor with a periodicity of 2.5 microns and a finger width near one micron.



(a) Optical micrograph  
(Nomarski) X320.

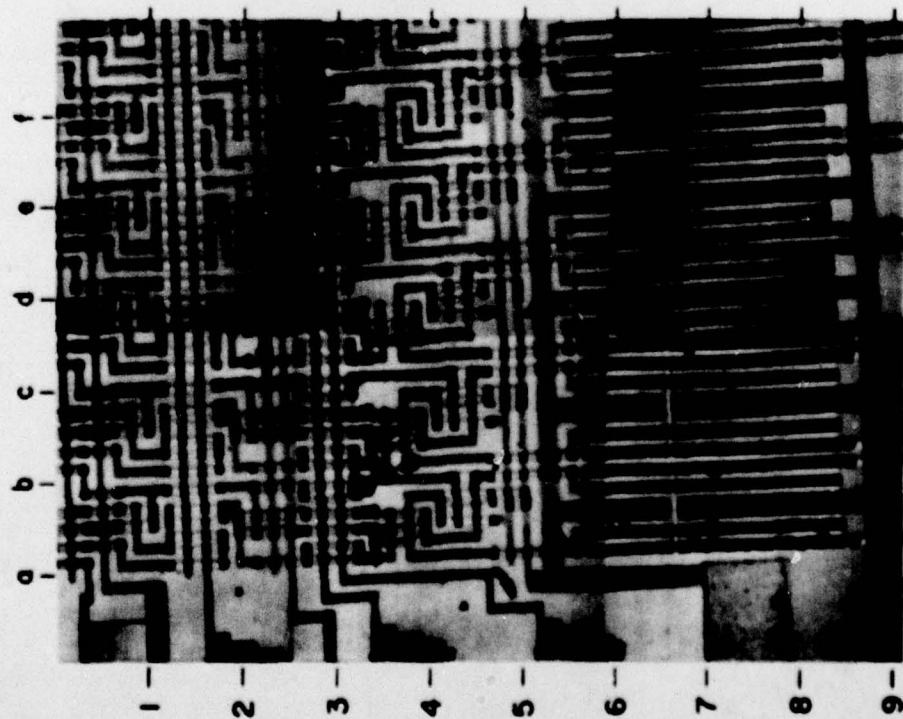
Fig.10a



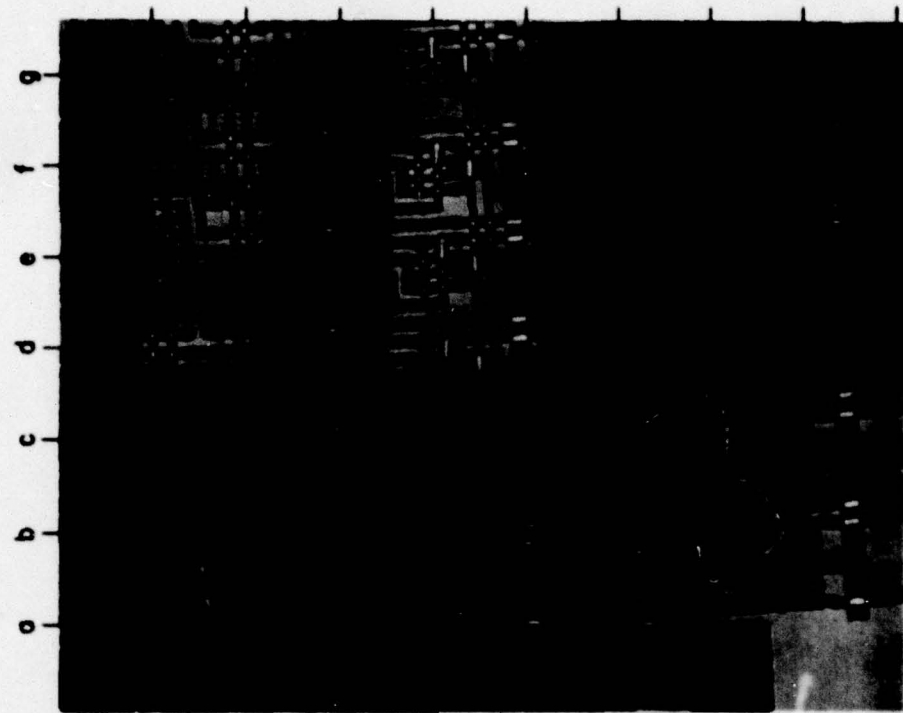
(b) Acoustic micrograph  
at X400.

Fig.10b

Integrated circuit fabricated on an SOS wafer.  
Note defect at the intersection of line C-C  
and 6-6.



(a) IN FOCUS



(b) SURFACE MOVED  $6\mu\text{m}$  TOWARD LENS FROM POSITION (a)

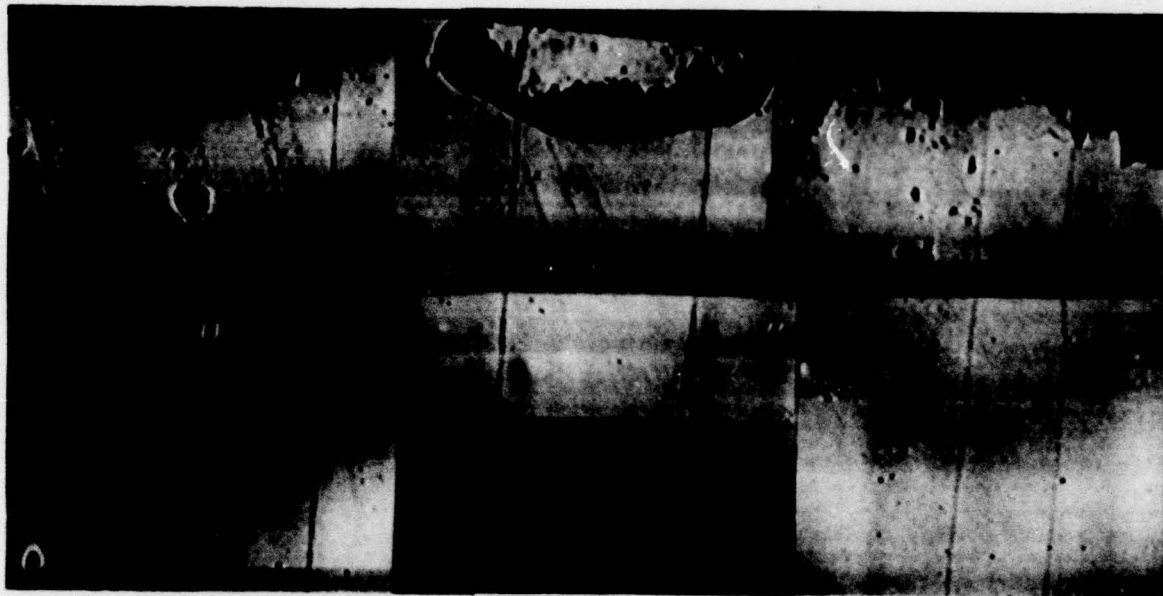
ACOUSTIC MICROGRAPHS OF INTEGRATED CIRCUIT ON  $\text{SiO}_2$   
(STDL-4)

The versatility of the new microscope was such that we thought it could be useful in examining structure and materials other than silicon. The optical and acoustic comparison of an epitaxial wafer of GaAs of Fig. 12 is an example of what it is that we want to do. The state of the art for the GaAs technology is not as advanced as that for silicon and as a result there are numerous defects in most wafers. It may represent an opportunity for acoustic microscopy.

The illustration of a single crystal of aluminum, as in Fig. 13, is a concrete example that indicates that we can observe subsurface damage. The horizontal lines are slip lines which were introduced intentionally by bending the crystal. The vertical lines are subsurface damage which comes from scratches that have not been completely eliminated in the final polishing. This is revealed in the SEM image. There the incident electrons penetrate the aluminum surface to a depth of about one micron.

In Fig. 14 we illustrate a case where the acoustic micrograph is taken in transmission. It reveals information that is not available in either the images from the optical instrument or the electron microscope. The object is a thin foil of tin about 12 microns in thickness. The diagonal lines in the acoustic image are visible on the surface. They result from the marks of the roller used in making the foil. But the dark spots are not visible on either surface. They appear to be inclusions of acoustically dense material within the interior of the foil.

In Fig. 15 we have another illustration of information that can be gathered with the acoustic microscope - information that is not available in the optical images. There we find an image of a polished surface of an alloy

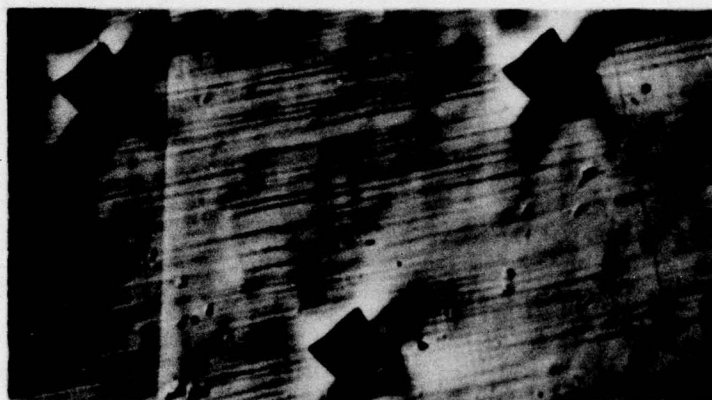


(a) ACOUSTIC x 200

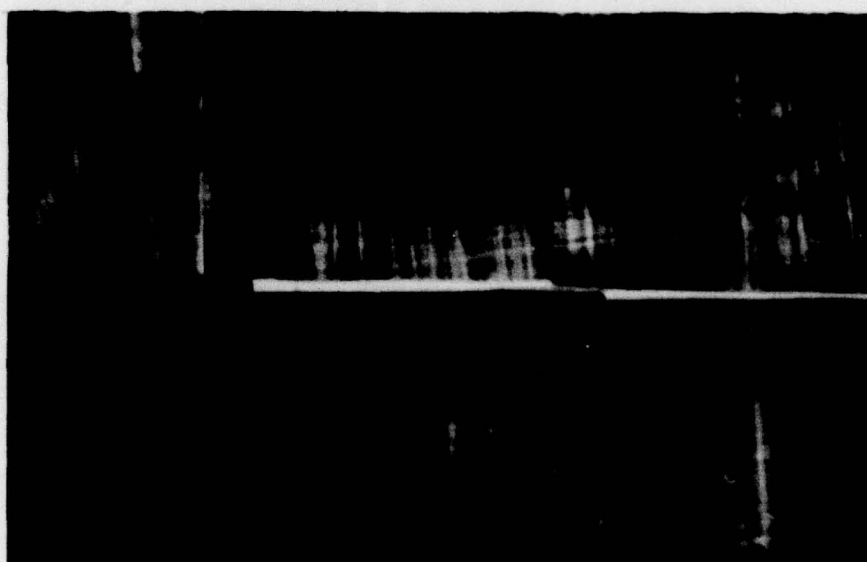


(b) OPTICAL x 100

Fig. 12 Epitaxial GaAs on GaAs substrate LPE with meniscus lines.



(a) OPTICAL (NOMARSKI) IMAGE  $\times 125$

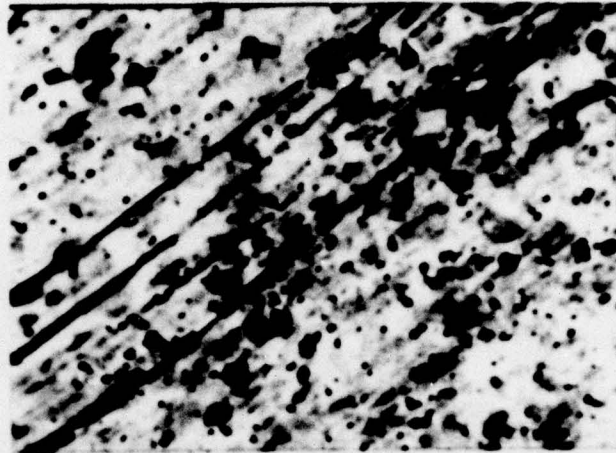


(b) ACOUSTIC IMAGE  $\times 150$

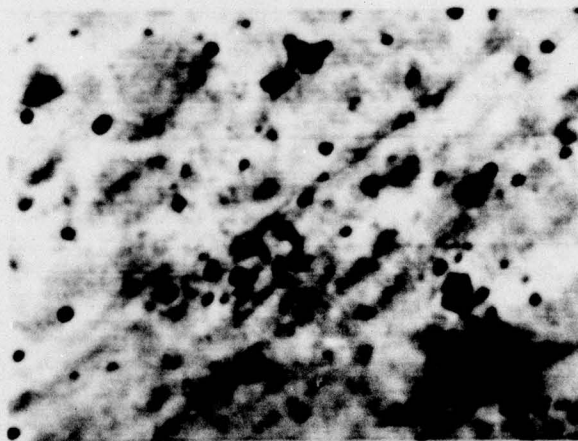


(c) SEM IMAGE  $\times 250$  [UPPER RIGHT  
INDENT OF (a) AND (b)]

Fig. 13 Surface of single crystal of aluminum bent to induce slip line.



(a) TINFOIL (12 MICRONS THICK)  
x 200

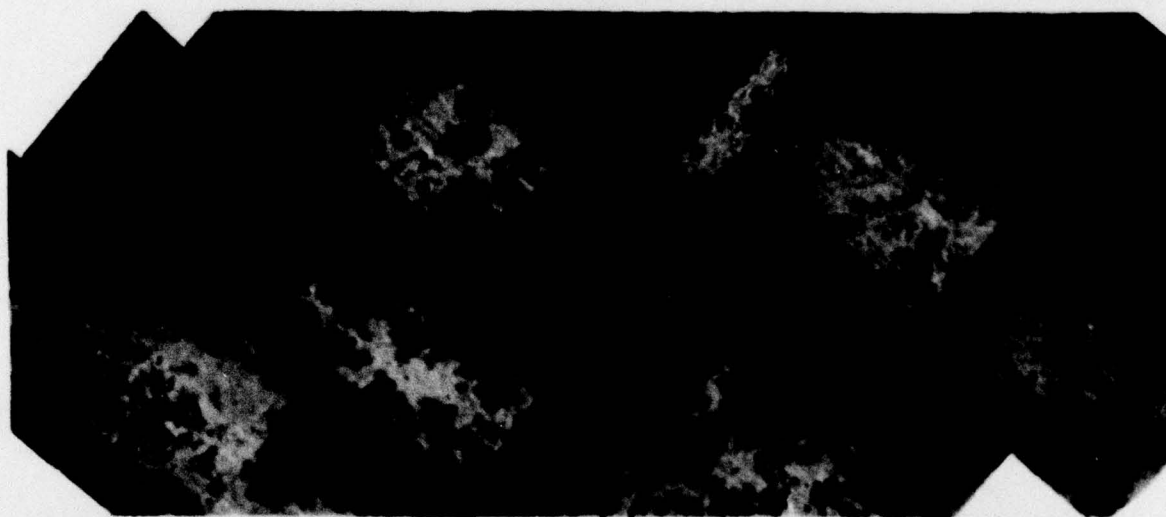


(b) TINFOIL (12 MICRONS)  
x 400

Fig. 14



(a)  
NOMARSKI  $\times$  250  
Co - Ti

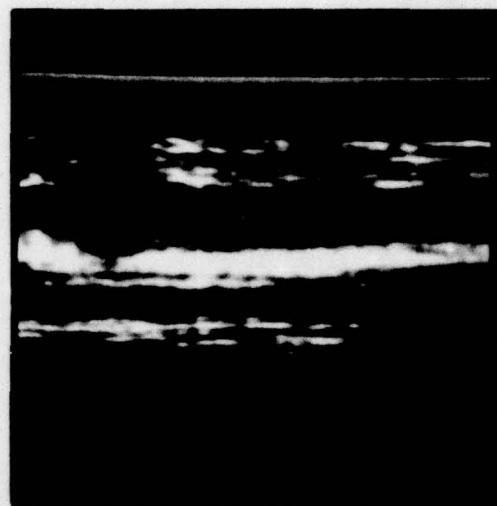
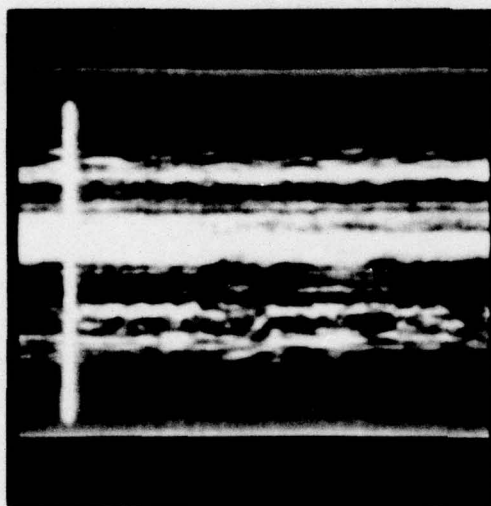


(b)  
ACOUSTIC  
Co - Ti

Fig. 15

of Cobalt and Titanium. The surface is marked with diamond points on the left and right to define the field of view. This alloy is a two-phase substance and in the acoustic micrograph (reflection) we observe the grey splotches which we interpret as regions of different compositions. We suspect that it is the difference in acoustic impedance of the different compositions that gives rise to the contrast that is visible in Fig. 15(b).

And, finally, in Fig. 16 we show a technique which differs from the direct images of the previous illustrations. This was taken in a transmission instrument. The object is an optical fiber as used in optical communication network. There we record the diffraction pattern of the beam after it has traversed the cylindrical lenses as formed by the fiber. The detail as found in a true image is not available but we do believe that mechanical inhomogeneities along the length can be easily detected in this type of display. This could be important in locating defects that lower the strength of the fiber.



OPTICAL GLASS FIBER -  $125\mu\text{m}$  DIAMETER  
ALUMINUM COATED

Fig. 16